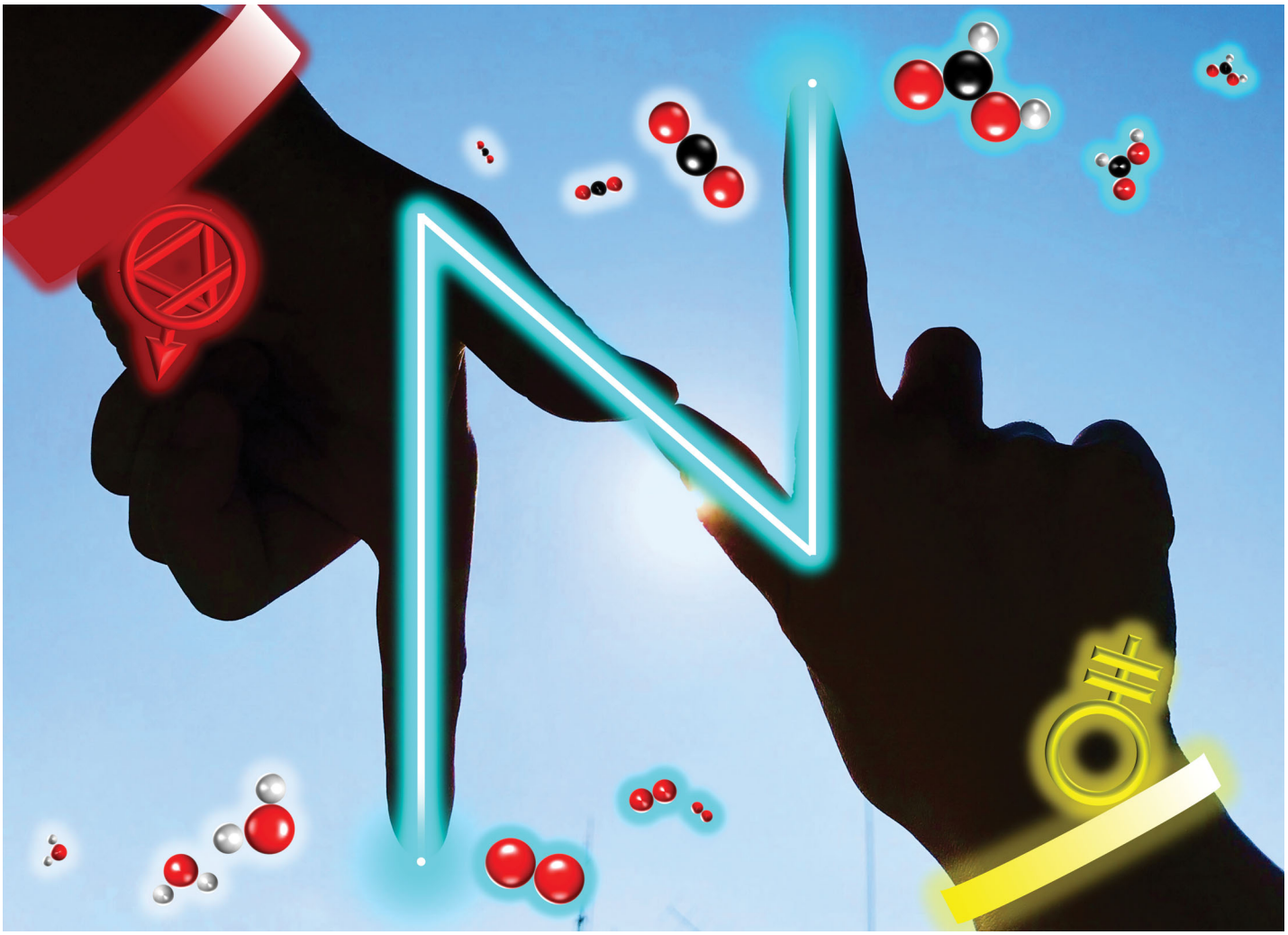

Showcasing collaborative research from Prof. Masahiro Miyauchi's group (Tokyo Institute of Technology, Japan) and Dr Hideki Abe's group (National Institute of Materials Science, Japan).

A Cu–Zn nanoparticle promoter for selective carbon dioxide reduction and its application in visible-light-active Z-scheme systems using water as an electron donor

An efficient Z-scheme system has been developed based on Cu–Zn nanoparticles modified light harvesting semiconductors. The system selectively converts CO_2 to HCOOH under visible light irradiation through water oxidation. Our system consists of robust, safe and inexpensive inorganic materials and is promising for a natural plant-like artificial photosynthesis.

As featured in:

See Hideki Abe, Masahiro Miyauchi *et al.*, *Chem. Commun.*, 2018, **54**, 3947.

ROYAL SOCIETY OF CHEMISTRY

rsc.li/chemcomm

Registered charity number: 207890

ChemComm

COMMUNICATION

View Article Online
View Journal | View Issue

Open Access Article. Published on 13 February 2018. Downloaded on 12/4/2025 7:41:09 PM.
This article is licensed under a Creative Commons Attribution 3.0 Unported Licence.

Check for updates

Cite this: *Chem. Commun.*, 2018, **54**, 3947

Received 22nd January 2018,
Accepted 13th February 2018

DOI: 10.1039/c8cc00535d

rsc.li/chemcomm

A Cu–Zn nanoparticle promoter for selective carbon dioxide reduction and its application in visible-light-active Z-scheme systems using water as an electron donor†

Ge Yin,[a] Hiroshi Sako,[a] Ramesh V. Gubbala,[b] Shigenori Ueda,[c] Akira Yamaguchi,[a] Hideki Abe*[b] and Masahiro Miyauchi*[a]

Selective carbon dioxide photoreduction to produce formic acid was achieved under visible light irradiation using water molecules as electron donors, similar to natural plants, based on the construction of a Z-scheme light harvesting system modified with a Cu–Zn alloy nanoparticle co-catalyst. The faradaic efficiency of our Z-scheme system for HCOOH generation was over 50% under visible light irradiation.

Artificial photosynthesis for fuel production from carbon dioxide (CO_2) and water (H_2O), driven by sunlight under moderate conditions, is a very attractive renewable energy strategy to solve the CO_2 emission issue.[1] Although numerous studies have reported water splitting to produce hydrogen (H_2),[2,3] photocatalytically reducing CO_2 into C1 molecules is more challenging, because it requires a higher reduction overpotential than proton reduction. Moreover, oxygen production is essential, since abundant water molecules should be used as electron donors for CO_2 reduction, similar to natural plants. However, many previous studies used sacrificial agents like triethanolamine (TEOA) or ethylenediaminetetraacetic acid (EDTA) to donate electrons.[4,5] To provide the high reduction potential and the strong oxidation power for photocatalytic CO_2 reduction through water oxidation, wide-gap semiconductors have been used to initiate CO_2 reduction under UV light irradiation, *i.e.* layered metal oxide perovskites ($BaLa_4Ti_4O_{15}$),[6] niobate nanosheets ($Nb_3O_8^-$),[7] or $SrTiO_3$.[8] However, visible-light-driven CO_2 photoreduction is more desirable because about half of solar energy ranges in the visible light range. It is very difficult for a narrow-band-gap light harvester material to provide the high reduction potential needed for CO_2 reduction as well as the deep oxidation potential for water oxidation.[9,10] To overcome the difficulties of using water as an electron donor and a visible light energy source, the Z-scheme system like the photosynthetic reaction centres in natural plants is useful and has previously been reported in the field of environmental purification[11] or water splitting.[12] Sekizawa *et al.* reported a Z-scheme system for photocatalytic CO_2 reduction by combining cathodic and anodic light harvesters.[13] Kudo *et al.* reported a metal sulfide/$BiVO_4$ Z-scheme using water as the electron donor,[14] and achieved the reduction of CO_2 into carbon monoxide (CO) under visible light. However, the produced H_2 amount was about 100 times higher than CO. Recently, Ishitani *et al.* also used a Z-scheme system for visible-light-driven CO_2 reduction, owing to the noble metal (Ru and Re) organic complex co-catalyst, and CO was selectively produced.[15] Its light-to-energy conversion efficiency, however, was still much smaller than that of natural plants. Besides CO, formic acid (HCOOH) is also very desirable C1 chemical for its general utilization in the fields of energy, chemical industry, and even animal husbandry.[16] To drive CO_2 reduction selectively into CO or HCOOH and to avoid hydrogen production in aqueous media, the co-catalyst modification onto the light harvester is crucial. However, highly selected HCOOH generation has only been achieved by using expensive noble metal-complexes to date.[17] In contrast, in our previous research, copper and zinc based bulk alloys were investigated as electrocatalysts for HCOOH production,[18] but they could not be applied in photocatalysis or photo-electrochemical systems because of their bulk form and/or high temperature preparation conditions.

Herein, we developed highly dispersed Cu–Zn alloy nanoparticles (NPs) *via* a moderate chemical co-reduction method and used them as a HCOOH generation promoter. The nanoparticles provide a high surface area to minimize the co-catalyst loading amount onto light harvesting semiconductors. A highly dispersed Cu–Zn NP ink enabled us to coat them onto various light harvesters. Based on these nanoparticles, we constructed a selective visible-light-driven CO_2 photoreduction system using water as an electron donor, consisting of robust and economical

[a] *Department of Materials Science and Engineering, School of Materials and Chemical Technology, Tokyo Institute of Technology, 2-12-1 Ookayama, Meguro-ku, Tokyo 152-8552, Japan. E-mail: mmiyauchi@ceram.titech.ac.jp*
[b] *Advanced Electronic Materials Center, National Institute of Materials Science, 1-1 Namiki, Tsukuba 305-004, Japan. E-mail: ABE.Hideki@nims.go.jp*
[c] *Synchrotron X-ray Station at SPring-8, National Institute for Materials Science, 1-1-1 Kouto, Sayo, Hyogo, 679-5148, Japan*

† Electronic supplementary information (ESI) available. See DOI: 10.1039/c8cc00535d

Open Access Article. Published on 13 February 2018. Downloaded on 12/4/2025 7:41:09 PM.
This article is licensed under a Creative Commons Attribution 3.0 Unported Licence.

inorganic components. As for the visible light harvesting system, a $CaFe_2O_4$ (CFO) film was used as the photocathode due to its high conduction band edge, ubiquitous elemental composition,[19,20] and high photo-current, which can be greatly improved by increasing its crystallinity.[19] On the other hand, an oriented WO_3 nanotree film was chosen as the photoanode, because it can be fabricated *via* facile hydrothermal treatment of a metal tungsten substrate with a large surface area and high crystallinity, and its quantum efficiency for water oxidation is quite high.[21] On the basis of each component, we constructed a Z-scheme system and evaluated its photocatalytic CO_2 reduction properties in the present study. Further, we conducted *operando* Fourier Transform Infrared Spectrometer (FT-IR) analysis to discuss the selective HCOOH production pathway on the Cu–Zn NPs' surface under real catalysis conditions.

Although our previous study reported the synthesis of the bulk Cu–Zn electrocatalyst for selective CO_2 reduction,[18] the present study developed the highly dispersed intermetallic Cu–Zn NPs *via* a wet chemical process and optimized their chemical composition and structure according to the performance of their electrochemical CO_2 reduction (described in the ESI† in detail, Fig. S3 and S4). Among various Cu/Zn ratios in NPs, the Cu_5Zn_8 phase exhibited the lowest onset potential for electrocatalytic CO_2 reduction (Fig. S5, ESI†). The optimal size of the Cu–Zn NPs was in the range of 20–40 nm (Fig. 1a). Hard X-ray photoelectron spectroscopy (HAXPES) analyses (Fig. 1b and c) were also performed, and the peak positions of the Cu 2p and Zn 2p core-levels were significantly shifted as compared to the pure Cu and Zn, indicating the formation of an intermetallic structure in the Cu–Zn alloy. The prepared Cu–Zn NPs were finely dispersed into an ink and could be coated onto various powder or film form electrodes by simple drop-casting or spin coating and a vacuum drying procedure at room temperature.

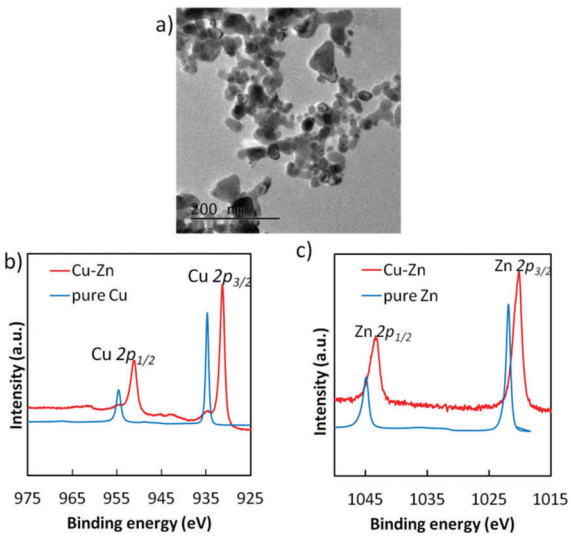

Fig. 1 (a) TEM image of Cu–Zn alloy nanoparticles. (b) HAXPES for Cu 2p and (c) Zn 2p core-levels in the prepared Cu–Zn alloy nanoparticles, compared to pure Cu and pure Zn.

Electrocatalytic selectivity for HCOOH generation of the Cu–Zn NP deposited electrode was very high (Fig. S8, ESI†). In addition to the electrocatalysis, we have confirmed that the Cu–Zn NPs act as a co-catalyst with UV-light-active $SrTiO_3$ with more than 50% selectivity for HCOOH generation (Fig. S9 and S10, ESI†).

To discuss the high selectivity of Cu–Zn NPs for HCOOH generation, *operando* FT-IR spectra were analyzed under the almost similar conditions to the real catalytic atmosphere under a humid CO_2 atmosphere with UV irradiation (Fig. S11 in the ESI†). As we can see in Fig. 2a, a peak appeared at 1409 cm^{-1}, while there were no peaks in the control groups (more control experiment results are shown in Fig. S12, ESI†). According to the literature, this peak can be assigned to bidentate carbonate[22] or bicarbonate,[23] whose appearances are commonly considered as the starting species of the HCOOH generation in CO_2 reduction.[24,25] In contrast, Cu was known for its high selectivity for CH_4 or CH_3OH. From the spectra of the Cu NP loaded photocatalyst in Fig. 2b, a peak which can be assigned to unidentate carbonate[22] or carboxylate[23] appeared at 1596 cm^{-1}. The results of *operando* FT-IR proved that the surface adsorption strength for CO_2* active species was adjusted by alloying on the atomic scale as we expected, thus the Cu–Zn NPs exhibited high selectivity for HCOOH generation.

As for the light harvesters to build a visible light sensitive system, a highly (*hk*0)-oriented CFO electrode was prepared by annealing in air (Fig. S13, ESI†),[19,20] whereas the highly oriented WO_3 nanotree film used in this study was grown on a tungsten substrate *via* a hydrothermal process (Fig. S15, ESI†).[21] Fig. 3 shows the UV-visible absorption spectra of the CFO and WO_3 electrodes, showing the bandgaps of CFO and WO_3 to be 2.5 and 2.6 eV, respectively, indicating that both are visible-light responsive. The broad absorption of WO_3 above 500 nm, shown in Fig. 3b, does not contribute to the photocurrent generation because it is attributed to trapped electrons, which have low reduction and oxidation potential and strong localization.[26,27]

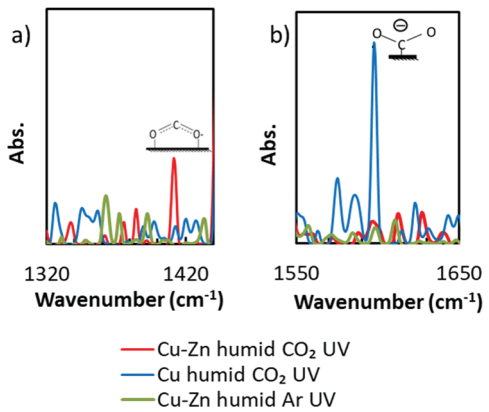

Fig. 2 The *operando* FT-IR spectra of photocatalyst powders loaded by Cu–Zn NPs and pure Cu NPs in a humid CO_2 atmosphere under UV irradiation. The spectra under humid Ar with UV irradiation are also shown as control groups. Strontium titanate was used as a photocatalyst powder. (a) and (b) show the spectra near 1400 cm^{-1} and 1600 cm^{-1}, respectively.

Open Access Article. Published on 13 February 2018. Downloaded on 12/4/2025 7:41:09 PM.
This article is licensed under a Creative Commons Attribution 3.0 Unported Licence.

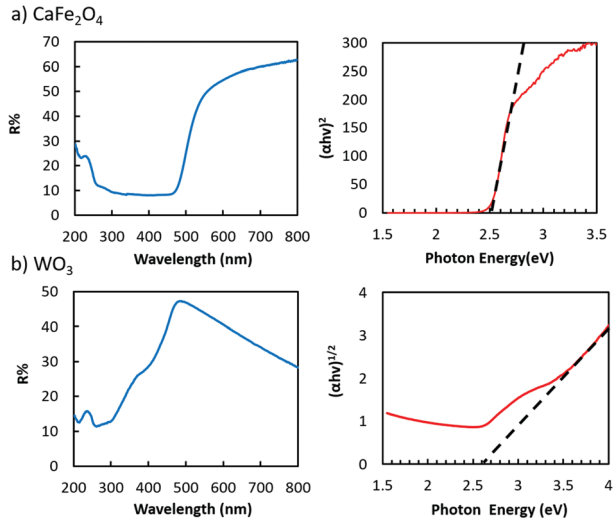

Fig. 3 UV-vis spectrum (a) plots of $(\alpha h\nu)^2$ *versus* photon energy of the pure $CaFe_2O_4$ (direct transition) electrode and (b) plots of $(\alpha h\nu)^{1/2}$ *versus* photon energy of the WO_3 (indirect transition) nanotrees electrode.

We deposited Cu–Zn NPs onto a CFO film by drop casting of a dispersed Cu–Zn NPs ink for selective CO_2 reduction. CO_2 was bubbled into an aqueous electrolyte solution surrounding the Cu–Zn/CFO electrode, whereas N_2 gas was purged into the WO_3 side electrolyte. The pH of the electrolytes was optimized based on the stability and performance of the photoelectrodes. The current–potential curves of the Cu–Zn/CFO and WO_3 electrodes are shown in Fig. 4. A cathodic photocurrent was observed at the Cu–Zn/CFO electrode, indicating that the CFO behaves as a p-type semiconductor. The potential threshold was about +0.6 V *vs.* Ag/AgCl, indicating that the valence band of the CFO was located around +1.22 V *vs.* the reversible hydrogen electrode (RHE) since the Fermi-level of p-type semiconductors would be close to the valence band position. Thus, the conduction band minimum is located around −1.27 V *vs.* RHE, which is enough negative potential to drive CO_2 reduction. On the other hand, the prepared WO_3 exhibited an anodic photocurrent, indicating the n-type photoanode behavior. The valence band position of WO_3 was calculated to be 3.35 V *vs.* RHE, suggesting that the WO_3 can oxidize water to O_2. On the basis of the photoelectrochemical half-cell properties shown in Fig. 4, our Z-scheme system can be expected to catalyze CO_2 reduction and generate O_2 from water in the CO_2 purged electrolyte as shown in the expected band-diagram in the ESI† (Fig. S1b). It is also noted that the photocurrent densities on the anodic and cathodic sides were balanced, which is very important to drive an efficient Z-scheme system.[28]

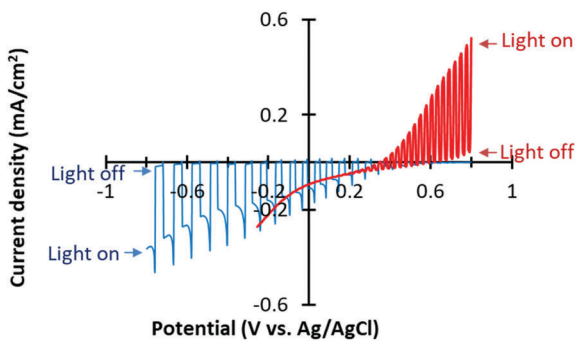

Fig. 4 Current–potential curves of the CFO electrode (blue) and WO_3 electrode (red) under chopped visible light irradiation. Electrolyte: 0.1 M $KHCO_3$ + 0.1 M KOH, CO_2 gas purged for the CFO electrode, pH = 7.2; 0.1 M KCl, N_2 gas purged for the WO_3 electrode, pH = 6.0.

The Z-scheme system was built using a Cu–Zn NPs modified CFO as the photocathode and WO_3 as the photoanode (see the schematic illustration, Fig. S1, ESI†). We applied a bias potential of −0.5 V onto the cathodic side, since only trace amounts of H_2 and C1 molecules were detected under the other potential conditions without any bias application (Fig. S16a, ESI†). CO_2 gas was bubbled in the cathodic side electrolyte and the anodic side was purged by N_2 to remove any dissolved oxygen. Without the Cu–Zn co-catalyst, hydrogen was preferably generated rather than C1 molecules in the cathodic side (Fig. S16b, ESI†). In contrast, the production of HCOOH was significant when the optimal amount of Cu–Zn NPs was coated onto the CFO surface (Fig. 5a). The result of selective HCOOH generation was reproducible (Fig. S17, ESI†) and the faradaic efficiency achieved for HCOOH generation was 53.6–56.1%. It should be noted that the produced amount of O_2 from the anodic side was almost half of the reduction products (Fig. 5b). For the generation of H_2, CO, and HCOOH molecules, two electrons are needed, while four electrons are donated from water to generate O_2. Therefore, it was proved that our Z-scheme system drives CO_2 reduction using water molecules as electron donors, similar to photosynthesis in natural plants.

This study is the first report to achieve highly selective HCOOH generation (>50%) from CO_2 photoreduction under visible light without the addition of sacrificial agents, based on inorganic robust materials. The turnover number (TON) of the Cu–Zn NPs in the present study was 12.35, even after 24 h of visible light irradiation, with a linear increase of HCOOH concentration. We have also confirmed that the Cu–Zn NPs remained stable even after 24 h photocatalytic evaluation according to our HAXPES analyses (Fig. S18, ESI†). Besides, the higher TON was recorded to be 1400 in the case of our Cu–Zn/$SrTiO_3$ under UV irradiation.[18] These results strongly suggest that our Z-scheme system is highly stable under photon irradiation in aqueous media.

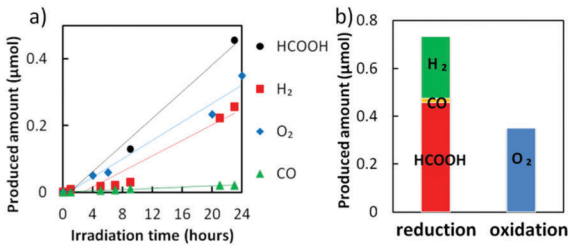

Fig. 5 (a) The produced amount of HCOOH, H_2, O_2 and CO from the Cu–Zn NPs loaded CFO/WO_3 system under visible light irradiation with a −0.5 V bias potential applied to the system. (b) The bar graph of the sum amount of the reduction products detected on the cathodic side and the O_2 detected from the anodic side after 24 h.

Open Access Article. Published on 13 February 2018. Downloaded on 12/4/2025 7:41:09 PM.
This article is licensed under a Creative Commons Attribution 3.0 Unported Licence.

The quantum efficiency for the reduction products was 0.14% in our system. Our light-to-energy conversion efficiency for the full xenon lamp spectrum was calculated to be 0.028%, which is 10 times higher than that of the previous pioneering work,[5] by considering the electrical bias and chemical bias from the pH difference between the cathode and the anode (see the ESI†). The cathodic surface improvement by Cu–Zn NPs was critical for the high performance of selectivity, efficiency and activity of the system. In addition, the Cu–Zn NPs proved to be a general co-catalyst which can be broadly applied to various kinds of light harvesters, due to their facile deposition under moderate conditions by using an ink method.

In conclusion, we have demonstrated that Cu–Zn alloy NPs can be utilized as a general CO_2 reduction catalyst, exhibiting high selectivity for HCOOH generation. A Z-scheme system constructed from a Cu–Zn NPs decorated highly crystallized $CaFe_2O_4$ photocathode and a WO_3 nanotree photoanode drove selective CO_2 photoreduction through water oxidation under visible light irradiation. Our system consists of robust inorganic materials and safe, inexpensive elements. The faradaic efficiency for HCOOH generation was over 50%, and the light energy conversion efficiency reached 0.028%. These results are promising for the development of a natural plant-like, visible-light-driven CO_2 photoreduction system.

This work was supported by Grants-in-Aid from the Advanced Catalytic Transformation Program for Carbon Utilization (ACT-C, Grant JPMJCR12ZG), Japan Science and Technology Agency (JST), and Japan Society for the Promotion of Science (JSPS) KAKENHI Grant Number 26410234 and 16J08808. The HAXPES measurements were performed with the approval of the NIMS Synchrotron X-ray Station (Proposal #2015A4603 and 2015B4605). We also appreciate preliminary research on WO_3 nanotrees by Mr Y. Nukui.

Conflicts of interest

There are no conflicts of interest to declare.

Notes and references

1 X. Chang, T. Wang and J. Gong, *Energy Environ. Sci.*, 2016, **9**, 2177–2196.
2 S. Chen, T. Takata and K. Domen, *Nat. Rev. Mater.*, 2017, **2**, 17050.
3 K. Iwashina, A. Iwase, Y. H. Ng, R. Amal and A. Kudo, *J. Am. Chem. Soc.*, 2015, **137**, 604–607.
4 T. M. Suzuki, T. Nakamura, S. Saeki, Y. Matsuoka, H. Tanaka, K. Yano, T. Kajino and T. Morikawa, *J. Mater. Chem.*, 2012, **22**, 24584–24590.
5 R. Kuriki, M. Yamamoto, K. Higuchi, Y. Yamamoto, M. Akatsuka, D. Lu, S. Yagi, T. Yoshida, O. Ishitani and K. Maeda, *Angew. Chem., Int. Ed.*, 2017, **56**, 4867–4871.
6 K. Iizuka, T. Wato, Y. Miseki, K. Saito and A. Kudo, *J. Am. Chem. Soc.*, 2011, **133**, 20863–20868.
7 G. Yin, M. Nishikawa, Y. Nosaka, N. Srinivasan, D. Atarashi, E. Sakai and M. Miyauchi, *ACS Nano*, 2015, **9**, 2111–2119.
8 S. Shoji, G. Yin, M. Nishikawa, D. Atarashi, E. Sakai and M. Miyauchi, *Chem. Phys. Lett.*, 2016, **658**, 309–314.
9 D. Scaife, *Sol. Energy*, 1980, **25**, 41–54.
10 S. Chen and L.-W. Wang, *Chem. Mater.*, 2012, **24**, 3659–3666.
11 Y.-C. Pu, W.-H. Lin and Y.-J. Hsu, *Appl. Catal., B*, 2015, **163**, 343–351.
12 J.-M. Li, H.-Y. Cheng, Y.-H. Chiu and Y.-J. Hsu, *Nanoscale*, 2016, **8**, 15720–15729.
13 K. Sekizawa, K. Maeda, K. Domen, K. Koike and O. Ishitani, *J. Am. Chem. Soc.*, 2013, **135**, 4596–4599.
14 A. Iwase, S. Yoshino, T. Takayama, Y. H. Ng, R. Amal and A. Kudo, *J. Am. Chem. Soc.*, 2016, **138**, 10260–10264.
15 G. Sahara, H. Kumagai, K. Maeda, N. Kaeffer, V. Artero, M. Higashi, R. Abe and O. Ishitani, *J. Am. Chem. Soc.*, 2016, **138**, 14152–14158.
16 E. Baytok, T. Aksu, M. A. Karsli and H. Muruz, *Turk. J. Vet. Anim. Sci.*, 2005, **29**, 469–474.
17 T. Arai, S. Sato and T. Morikawa, *Energy Environ. Sci.*, 2015, **8**, 1998–2002.
18 G. Yin, H. Abe, R. Kodiyath, S. Ueda, S. Nagarajan, A. Yamaguchi and M. Miyauchi, *J. Mater. Chem. A*, 2017, **5**, 12113–12119.
19 S. Ida, K. Yamada, T. Matsunaga, H. Hagiwara, Y. Matsumoto and T. Ishihara, *J. Am. Chem. Soc.*, 2010, **132**, 17343–17345.
20 Y. Matsumoto, M. Obata and J. Hombo, *J. Phys. Chem.*, 1994, **98**, 2950–2951.
21 Y. Nukui, N. Srinivasan, S. Shoji, D. Atarashi, E. Sakai and M. Miyauchi, *Chem. Phys. Lett.*, 2015, **635**, 306–311.
22 H. Du, C. T. Williams, A. D. Ebner and J. A. Ritter, *Chem. Mater.*, 2010, **22**, 3519–3526.
23 K. K. Bando, K. Sayama, H. Kusama, K. Okabe and H. Arakawa, *Appl. Catal., A*, 1997, **165**, 391–409.
24 R. Kortlever, J. Shen, K. J. P. Schouten, F. Calle-Vallejo and M. T. Koper, *J. Phys. Chem. Lett.*, 2015, **6**, 4073–4082.
25 R. P. S. Chaplin and A. A. Wragg, *J. Appl. Electrochem.*, 2003, **33**, 1107–1123.
26 A. Kondo, G. Yin, N. Srinivasan, D. Atarashi, E. Sakai and M. Miyauchi, *Nanoscale*, 2015, **7**, 12510–12515.
27 Z. G. Zhao, Z. F. Liu and M. Miyauchi, *Adv. Funct. Mater.*, 2010, **20**, 4162–4167.
28 N. Srinivasan, E. Sakai and M. Miyauchi, *ACS Catal.*, 2016, **6**, 2197–2200.

 This journal is © The Royal Society of Chemistry 2018